

Reanalysis of the GALLEX solar neutrino flux and source experiments[†]

F. Kaether*, W. Hampel, G. Heusser, J. Kiko, T. Kirsten

Max Planck Institute for Nuclear Physics, P.O. Box 103980, D-69029 Heidelberg, Germany

Abstract

After the completion of the gallium solar neutrino experiments at the Laboratori Nazionali del Gran Sasso (GALLEX: 1991-1997; GNO: 1998-2003) we have retrospectively updated the GALLEX results with the help of new technical data that were impossible to acquire for principle reasons before the completion of the low rate measurement phase (that is, before the end of the GNO solar runs). Subsequent high rate experiments have allowed the calibration of absolute internal counter efficiencies and of an advanced pulse shape analysis for counter background discrimination. The updated overall result for GALLEX (only) is $73.4^{+7.1}_{-7.3}$ SNU. This is 5.3% below the old value of $77.5^{+7.5}_{-7.8}$ SNU [1], with a substantially reduced error. A similar reduction is obtained from the reanalysis of the ^{51}Cr neutrino source experiments of 1994/1995.

Key words: Solar Neutrinos, Gallium experiment, GALLEX, neutrino mass

PACS: 26.65.+t, 14.60.Pq

1. Introduction

The GALLEX detector at the Gran Sasso Underground Laboratory (LNGS) in Italy has monitored solar neutrinos with energies above 233 keV from 1991 to 1997 by means of the inverse β -decay reaction $^{71}\text{Ga}(\nu_e, e^-)^{71}\text{Ge}$ [1][2][3][4][5]. Together with the subsequent GNO experiment solar neutrinos have been recorded from 1991 to 2003, with a break in 1997 [6][7]. The experimental procedure for a typical GALLEX or GNO solar neutrino run has been as follows: 30.3 t of gallium in the form of a concentrated $\text{GaCl}_3\text{-HCl}$ solution are exposed to solar neutrinos for a time period between three and four weeks. In the solution, the neutrino-induced ^{71}Ge atoms as well as the inactive Ge carrier atoms added to the solution at the beginning of a run form the volatile compound GeCl_4 , which at the end of an exposure is swept out of the solution by means of a nitrogen gas stream. The nitrogen is then passed through a gas scrubber where the GeCl_4 is absorbed in water. The GeCl_4 is finally converted to GeH_4 which together with xenon is introduced into a proportional counter to determine the

number of ^{71}Ge atoms by observing their radioactive decay (half-life 11.43 d [8]).

In order to reduce the background in ^{71}Ge counting with proportional counters the pulses recorded by the data acquisition system were analyzed by a pulse shape discrimination method. In contrast to GNO, the published GALLEX data have so far been analyzed with a rather simple procedure, where pointlike ionizations are distinguished from extended background events by the time in which the proportional counter signal rises from 10% to 70% of the amplitude recorded by the transient digitizer. A more sophisticated method has been developed [9][10][11] and tested already in GALLEX [12]. However, in order to determine the cut efficiency for such a procedure, a calibration data set with high statistics measured with the full counting system is required. In order not to damage the low counter backgrounds, such data could only be acquired at the very end of GALLEX in the frame of the ^{71}As experiment [13], in which a rather large number of ^{71}Ge decays ($\sim 10^4$) has been recorded. Using this data set, a new pulse shape discrimination method has now been developed and applied to the GALLEX data [14].

There are two additional motivations to reanalyse the GALLEX solar neutrino data as well as the data from the two ^{51}Cr neutrino source experiments that were performed in GALLEX [15][16]. At first, 10 out of 22 coun-

*Corresponding author. Tel.: +49 6221 516828
 Email address: Florian.Kaether@mpi-hd.mpg.de (F. Kaether)

[†]Dedicated to Michael Altmann, Nicola Ferrari and Keith Rowley.
 Accepted by *Physics Letters B*, January 13, 2010

ters used in the GALLEX solar neutrino measurements and 4 out of 14 counters used in the GALLEX ^{51}Cr neutrinos source experiments have been absolutely calibrated in the frame of the GNO experiment [7][17]. Secondly, there is now an improved value for the solar neutrino signal and its error available which has to be subtracted from the measured signal in the analysis of the ^{51}Cr data.

2. Pulse shape analysis in ^{71}Ge counting

^{71}Ge decays back to ^{71}Ga by K, L or M electron capture. The hole in the corresponding shell is filled by transitions of electrons from higher shells. The released energy is mostly transferred to electrons from the same or higher shells which subsequently are emitted as Auger-electrons. Only in the case of L to K transitions a substantial fraction of cases leads to the emission of a K-alpha X-rays (9.3 keV) because of the rather high fluorescence yield of the K shell (0.528). The range of Auger-electrons in the counter gas is rather small (< 1 mm) and therefore the volume extension of the energy deposition is always small. On the other hand, the mean free path of a 9.3 keV X-ray is about 1 cm and hence similar to the counter dimensions. The X-ray is therefore either able to leave the counter undetected or to produce a second separated energy deposit where the ratio of the two energies is at a fixed value of ≈ 8 . Neglecting M events (which are below the selected energy threshold) this leads to three different kinds of events: (a) a single electron cloud corresponding to an energy of 10.4 keV, (b) a single electron cloud of about 1.2 keV, and (c) two electron clouds of 1.1 keV and 9.3 keV, respectively. Contrary, background events are mainly caused by higher energy electrons coming from beta decays or they are induced by gamma rays via Compton effect. These events don't produce pointlike ionizations but an ionization track in the counting gas which leads to a slower rise time of the signals. An identification of pointlike ionizations, double ionizations or extended (multiple) events therefore allows to distinguish in many cases between ^{71}Ge decays and background events.

The new pulse shape discrimination method described here is performed in three steps. At first, the original pulses are slightly smoothed. This is necessary due to electrical and digital noise affecting the pulse shape, particularly for low energy events. A piecewise polynomial fit was used. For each data point $P(t_i)$ a region of $t_i \pm 8$ ns (corresponding to 20 data points on each side) was fitted with a second order polynomial $p(t)$. Finally each data point $P(t_i)$ was replaced by $p(t_i)$. This method has the advantage that it provides an adequate

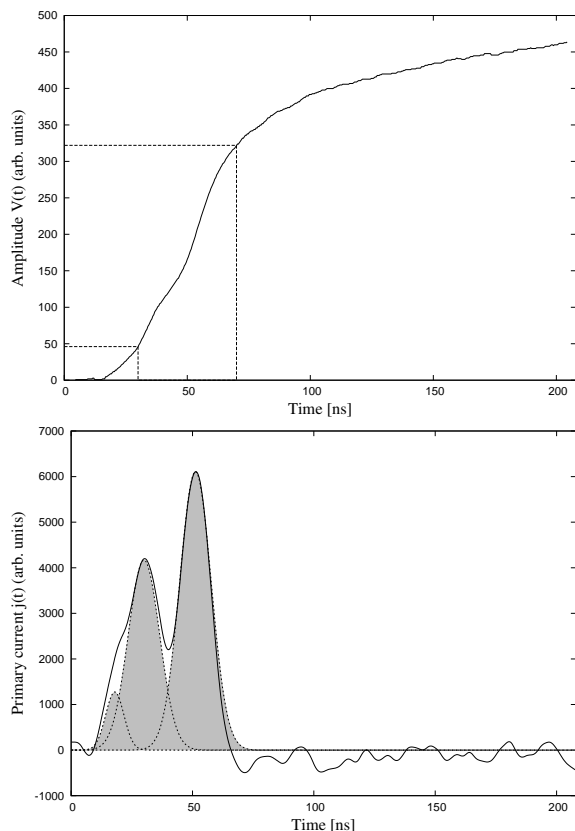


Figure 1: Proportional counter signal $P(t)$ of a typical multiple event in addition with the 10%-70% rise time levels (above) and the primary current $j(t)$ of the same event derived by deconvolution with the three major peaks (below).

noise reduction but conserves even sharp structures on bigger time scales.

A pointlike energy deposition in the counter leads to a cloud of primary electrons which is δ -shaped (neglecting diffusive effects) when reaching the gas amplification zone in the proportional counter. Under ideal conditions (perfect radial electric field, constant ion mobility) the shape of the resulting preamplifier output pulse can be written as $P_\delta(t) = V_0 \log(1 + t/t_0)$ [12]. A general pulse shape can then be described by a convolution of the pulse shape caused by a pointlike charge cloud with a function $j(t)$ which parameterises the number of electrons arriving at the gas amplification zone as a function of time: $P(t) = P_\delta(t) \otimes j(t)$. In order to reveal $j(t)$ from a measured pulse $P(t)$ one has to numerically deconvolute $P_\delta(t)$ from $P(t)$. This is the second step in the applied pulse shape analysis and is performed by a Fourier analysis (i.e. transforming the measured pulse into the frequency domain) where deconvolution is simply a division (for more details see [14]).

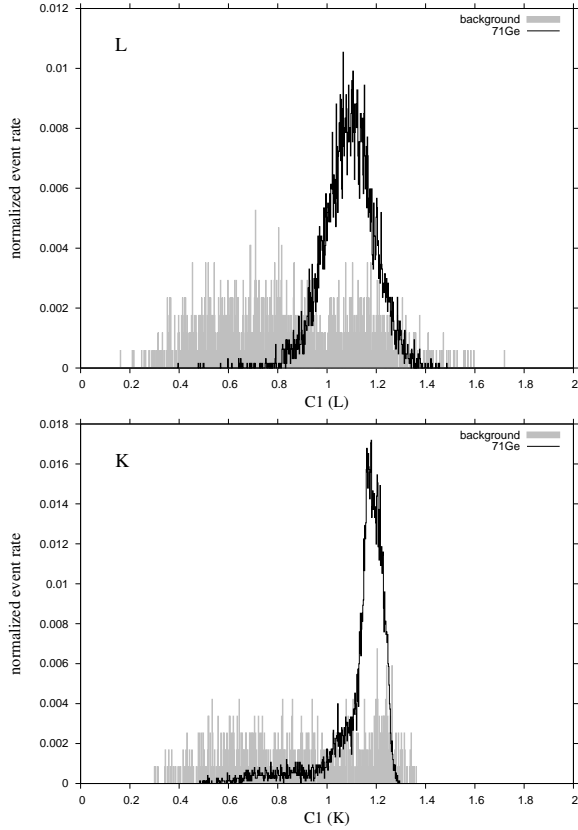


Figure 2: Distribution of pulse shape parameter C_1 for ^{71}Ge events (black) and background events (grey) in the L (above) and K (below) energy range.

An example of a typical multiple background event is shown in Figure 1 where the measured signal $P(t)$ and the primary current $j(t)$ derived by deconvolution is shown in the upper and lower figure, respectively. $j(t)$ is directly connected to the radial charge distribution in the proportional counter and each peak is caused by one single charge cloud. Identification of the major peaks of $j(t)$ (see lower part of Figure 1) is the third step in pulse shape analysis and is performed as follows:

- Determination of the maximum position t_{\max} .
- Determination of the full width at half maximum (FWHM). In cases of asymmetry on each side the half width was determined and the smaller value was chosen.
- The peak was approximated as a Gaussian $g(t_{\max}, \sigma)$ where $\text{FWHM} = 2.35\sigma$.
- Subtraction of Gaussian and repeat the procedure.

The resolution of this peak search algorithm was defined as follows: if the distance between the maxima of two

peaks was smaller than the mean of the half widths both peaks were combined into a single peak. Regarding Figure 1, the distance of the two leftmost peaks is slightly above the resolution threshold.

The total deposited energy is proportional to the number of primary charges and therefore to the total integral $\int j(t) dt$. The fraction C_i of energy deposited in one single charge cloud is therefore given by the peak integral normalised with the total energy

$$C_i = \frac{\int g(t_{\max}, \sigma) dt}{\int j(t) dt}. \quad (1)$$

For single events, where the energy deposit is concentrated in one single charge cloud, one expects a ratio of $C_1 \approx 1$ while C_2 and C_3 are caused by noise and therefore are small. Actually C_1 is often even slightly larger than 1 due to the fact that the negative noise part decreases $\int j(t) dt$. In contrast, for multiple events, C_1 is obviously smaller than 1 with a simultaneous increase of C_2 and C_3 . In the case of K double events one expects to recover the given ratio $C_1/C_2 \approx 8$.

Following these expectations, criteria for event selection were defined. To decide whether a parameter is suitable to distinguish background from ^{71}Ge events one needs reference pulses for both kinds of events. A sample of background events can be obtained from the solar runs themselves, since each sample was measured for about 180 days, but after 50 days ($\approx 3\tau$) the ^{71}Ge atoms initially present are decayed away.

A large amount of ^{71}Ge events were provided by the arsenic experiment [13] allowing to collect the parameter distribution with good statistics. Figure 2 shows the distributions of parameter C_1 for ^{71}Ge decays and background events. It is obvious that an adequate constraint on C_1 allows to select ^{71}Ge decays and to reject a large part of background events.

Finally, a comparison with events from calibrations with an external X-ray source (cerium) which were performed for all solar runs [2] provides the individual pulse shape parameter bounds for each run and a precise determination of the pulse shape cut efficiencies. The C_1 distribution for cerium events is very similar to germanium events. For each calibration the location and width of the C_1 -peak is estimated and an acceptance window for ^{71}Ge events is defined. The efficiency of this cut was determined using the arsenic runs for L events to $\varepsilon_L = 0.960 \pm 0.006$. The efficiency for K events is about 80% due to the fact that the C_1 cut rejects nearly all of the double events. To increase the number of accepted K double events an additional cut was defined using the ratio C_1/C_2 . Due to the limited energy resolution of

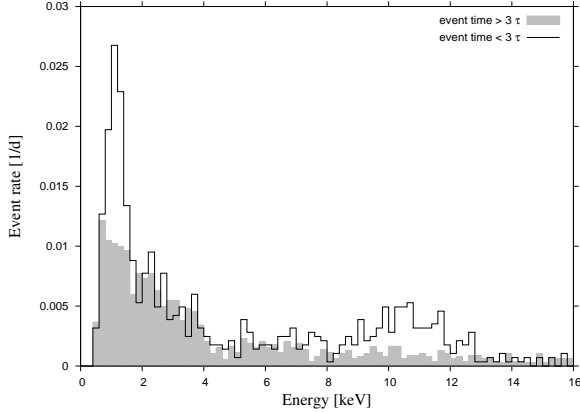


Figure 3: All candidate events, divided in early ($t < 3\tau$) and late ($t > 3\tau$) events.

the proportional counters a wide acceptance range for this ratio has been chosen ($5 < C_1/C_2 < 12$). To reject multiple background events with a ratio of C_1/C_2 within these bounds, an additional upper limit for C_3 was defined. Altogether one obtains an efficiency for K events of $\varepsilon = 0.861 \pm 0.018$. For more details see [14].

3. Solar run analysis

3.1. Event selection

In a first step, all obvious background events are removed by several cuts. These cuts are identical to those described in [2], except for the pulse shape cut, which was applied according to the procedure described in the previous section.

All remaining candidate events (without energy cut) are plotted in Figure 3, divided into early ($t < 3\tau$) and late events. The characteristics of a typical ^{71}Ge energy spectrum with the two peaks at 1.2 and 10.4 keV, respectively, are quite obvious in the early spectrum (solid line). The peak positions and widths as well as the intensities of both peaks are lying within the expected ranges.

3.2. Maximum Likelihood Analysis

The final cut to the data is the energy cut, by which only events are selected which are inside the L and K energy windows (see [2]). After this cut there remain 726 and 452 events for the L and the K energy window, respectively. These events were used for a maximum likelihood analysis which was described in [18] for the chlorine experiment and was adapted for GALLEX and GNO. The total production rate P of ^{71}Ge is

$$P = P_{\odot}/d_r^2 + P_{\text{fix}} \quad (2)$$

Efficiencies [7]	$\pm 2.6\%$
Energy cut [2]	$\pm 2.0\%$
Pulse shape analysis	$\pm 2.0\%$
Chemical yield [1]	$\pm 2.1\%$
Target mass [3]	$\pm 0.8\%$
^{68}Ge correction [1]	$+0.9\%$ -2.6%
Side reactions [1][19][20]	$\pm 1.5\%$
Rn cut [1]	$\pm 1.5\%$
Sum	$+5.0\%$ -5.6%

Table 1: Systematic error contributions

where P_{\odot} is the solar production rate which has to be corrected by the individual Earth-Sun distance for each run d_r (given in units of 1 AU), and $P_{\text{fix}} = (0.039 \pm 0.011)$ atoms per day which is a fixed component caused by side reactions (see [5]). P_{\odot} is one of the free parameters of the likelihood function \mathcal{L} . In addition one assumes the background rates in the two energy windows b_L and b_K as independent free parameters for each of the 65 GALLEX runs. Altogether the likelihood function has to be maximised for 131 free and independent parameters. This is done by using the Fortran library MINUIT provided by CERN to minimise $-\log \mathcal{L}$. The combined result for all GALLEX runs is

$$P_{\odot} = \left[73.4_{-6.0}^{+6.1} (\text{stat.})_{-4.1}^{+3.7} (\text{syst.}) \right] \text{ SNU} . \quad (3)$$

The statistical error determination is given in maximum likelihood theory by a variation of \hat{P}_{\odot} until

$$\log \mathcal{L}_{\text{max}} - \log \mathcal{L}(\hat{P}_{\odot}) = \frac{1}{2} \quad (4)$$

while $\log \mathcal{L}(\hat{P}_{\odot})$ was maximised regarding the remaining free parameters which leads to $1\sigma = P_{\odot}(\mathcal{L}_{\text{max}}) - \hat{P}_{\odot}$. A possible asymmetry of the error is considered by investigation of both sides of \mathcal{L}_{max} .

The systematic error includes the uncertainty of counter efficiencies, which decreased to 2.6% due to the more precise calibrations [7]. The error of the pulse shape cut efficiency was estimated to 2.0%. The contribution of other components are unchanged compared to previous publications, a compilation is given in Table 1.

For the maximum likelihood analysis the half-life of ^{71}Ge is usually fixed to its known value of 11.43 d. However, it can also be treated as an additional free parameter. This yields 10.3 ± 1.2 d, which is in agreement with the expected value. Moreover, due to the radon cut inefficiency and the short half-life of ^{222}Rn and its

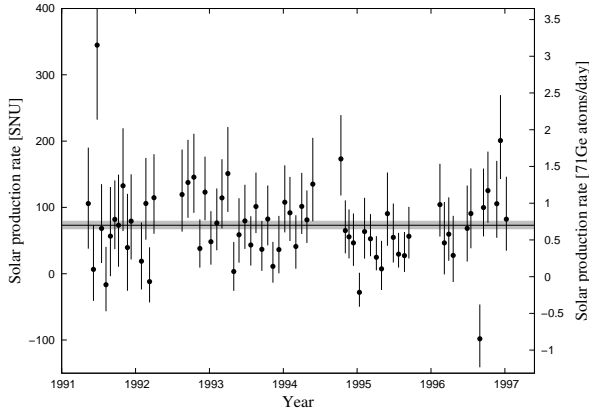


Figure 4: Single results of the 65 GALLEX solar runs (error bars are $\pm 1\sigma$ statistical).

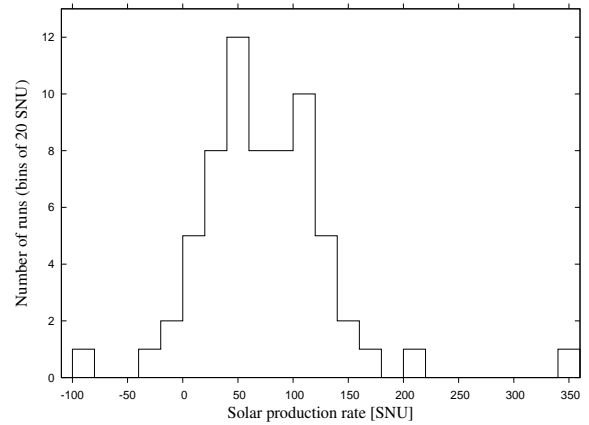


Figure 5: Distribution of the GALLEX single run results in bins of 20 SNU.

daughters one expects a small bias towards a shorter half-life. Besides the energy spectrum characteristics, this is a strong proof of the GALLEX data set consistency.

For a comparison with the previously published results we repeated the rise time analysis. The event selection procedure described in section 3.1 was used identically except the pulse shape analysis was replaced by the rise time method. The new counter efficiencies were considered as well as the correction due to the earth-sun distance variation (which so far had not been applied in the GALLEX data analysis). The result

$$P_{\odot}^{\text{RT}} = \left[77.4_{-6.2}^{+6.4} (\text{stat.})_{-4.3}^{+3.9} (\text{syst.}) \right] \text{ SNU} \quad (5)$$

is in very good agreement with the value of $\left[77.5 \pm 6.2 (\text{stat.})_{-4.7}^{+4.3} (\text{syst.}) \right] \text{ SNU}$ given in [1]. All changes average to near zero, except for the pulse shape analysis.

3.3. Single runs and GALLEX I-IV

The single run results are listed in Table 3 and Table 4 and are plotted in Figure 4. The histogram in Figure 5 shows the distribution of results in bins of 20 SNU.

Even though the statistical error of a single run result is usually asymmetric, one expects a normal distribution as shown by Monte Carlo simulations [1]. This expectation was tested by a Kolmogorow-Smirnov-test. The test value is defined as the maximum deviation D between the cumulative distribution functions of the given data set and the expected normal distribution. One obtains $D = 0.076$ for the GALLEX data set. For randomly generated samples one gets higher values of D in 54% of all cases and a 90% confidence level of $D_{90} = 0.1$. For a second test (which is related to the latter one but more sensitive concerning outliers) the test value was defined

as the total integral of absolute deviations between the cumulative distribution functions. In 19% of cases randomly generated samples created higher values than the original data set. From these points of view there is no reason to doubt the hypothesis of a normal distribution.

The statistical errors of single runs are rather big, because even a single accepted or rejected event is able to change the result of a run by 10 SNU or even more. Therefore a run by run comparison between pulse shape and rise time analysis is not very meaningful. Only combinations of many runs are suitable to provide enough statistics to decrease the error to a significant level. Therefore the 65 runs were sorted into groups. For historical reasons we stayed with the grouping in four periods of data taking which occurred in a natural way by interruptions for construction works or source experiments. Nevertheless, this kind of grouping is arbitrary and should have no effect on the results.

The results of the four GALLEX periods are shown in Figure 6 and are listed in Table 2 with rise time and pulse shape analysis, respectively. While the results of

GALLEX period	Results [SNU]	
	rise time	pulse shape
I	$84.0_{-16.7}^{+17.6}$	$75.1_{-16.2}^{+17.3}$
II	$77.2_{-9.5}^{+9.9}$	$82.8_{-9.5}^{+10.0}$
III	$51.2_{-10.0}^{+10.8}$	$49.5_{-9.8}^{+10.7}$
IV	$122.1_{-17.5}^{+18.4}$	$89.2_{-15.5}^{+16.6}$

Table 2: Results of the GALLEX periods I-IV with rise time and pulse shape analysis. The errors are 1σ (stat.).

GALLEX I		Exposure		pulse shape analysis		
Runs		start	duration (d)	b_L	b_K	P_\odot (SNU)
1	b29	14-MAY-1991	21.0	0.028	0.000	105^{+84}_{-68}
2	b31	5-JUN-1991	20.8	0.020	0.034	6^{+67}_{-47}
3	b32	26-JUN-1991	21.0	0.115	0.057	344^{+128}_{-112}
4	b33	17-JUL-1991	21.0	0.079	0.000	66^{+67}_{-52}
5	b34	7-AUG-1991	21.0	0.064	0.043	-17^{+57}_{-40}
6	b35	28-AUG-1991	22.3	0.035	0.024	56^{+74}_{-60}
7	b36	19-SEP-1991	19.7	0.000	0.000	82^{+59}_{-45}
8	b38	10-OCT-1991	19.9	0.068	0.059	73^{+76}_{-63}
9	b39	30-OCT-1991	21.0	0.058	0.003	133^{+87}_{-68}
10	b41	21-NOV-1991	19.9	0.218	0.114	40^{+81}_{-65}
11	b42	11-DEC-1991	28.0	0.098	0.010	80^{+71}_{-58}
12	b45	29-JAN-1992	21.0	0.034	0.032	19^{+58}_{-43}
13	b47	20-FEB-1992	19.8	0.028	0.020	106^{+69}_{-54}
14	b49	12-MAR-1992	18.8	0.092	0.000	-12^{+52}_{-31}
15	b50	31-MAR-1992	29.0	0.008	0.018	115^{+66}_{-54}
GALLEX II		Exposure		pulse shape analysis		
Runs		start	duration (d)	b_L	b_K	P_\odot (SNU)
16	a59	19-AUG-1992	28.0	0.046	0.018	120^{+68}_{-56}
17	a61	17-SEP-1992	27.0	0.034	0.019	138^{+64}_{-53}
18	a63	15-OCT-1992	27.0	0.059	0.016	146^{+66}_{-54}
19	a65	12-NOV-1992	27.0	0.038	0.000	38^{+44}_{-29}
20	a67	10-DEC-1992	27.0	0.000	0.000	123^{+54}_{-42}
21	a69	7-JAN-1993	27.0	0.051	0.021	48^{+46}_{-35}
22	a71	4-FEB-1993	27.0	0.083	0.037	77^{+52}_{-41}
23	a73	4-MAR-1993	29.0	0.016	0.012	114^{+58}_{-46}
24	a75	3-APR-1993	25.0	0.035	0.024	151^{+70}_{-58}
25	a77	29-APR-1993	27.0	0.044	0.038	3^{+44}_{-29}
26	a79	27-MAY-1993	27.0	0.036	0.026	59^{+55}_{-42}
27	a81	24-JUN-1993	27.0	0.040	0.017	80^{+54}_{-42}
28	a83	22-JUL-1993	27.0	0.057	0.006	43^{+43}_{-31}
29	a85	19-AUG-1993	27.0	0.014	0.006	101^{+51}_{-40}
30	a87	16-SEP-1993	27.0	0.029	0.042	37^{+43}_{-33}
31	a89	14-OCT-1993	27.0	0.019	0.038	82^{+51}_{-40}
32	a91	11-NOV-1993	27.0	0.042	0.025	11^{+37}_{-25}
33	a93	9-DEC-1993	27.0	0.014	0.021	37^{+51}_{-36}
34	a95	6-JAN-1994	27.0	0.024	0.011	108^{+56}_{-45}
35	a97	3-FEB-1994	27.0	0.032	0.018	92^{+54}_{-42}
36	a99	3-MAR-1994	27.0	0.021	0.010	41^{+47}_{-34}
37	a101	31-MAR-1994	27.0	0.034	0.014	102^{+51}_{-41}
38	a103	28-APR-1994	27.0	0.056	0.014	81^{+44}_{-35}
39	a105	26-MAY-1994	27.0	0.036	0.020	135^{+70}_{-56}

Table 3: Single solar run results with stat. error (1σ) for GALLEX I and II.

GALLEX III		Exposure		pulse shape analysis		
Runs		start	duration (d)	b_L	b_K	P_\odot (SNU)
40	a119	12-OCT-1994	21.0	0.058	0.011	173^{+66}_{-55}
41	a120	2-NOV-1994	21.0	0.031	0.007	65^{+46}_{-34}
42	a121	23-NOV-1994	21.0	0.028	0.010	56^{+41}_{-32}
43	a123	15-DEC-1994	27.0	0.039	0.036	47^{+44}_{-35}
44	a124	11-JAN-1995	28.0	0.079	0.049	-28^{+30}_{-22}
45	a125	8-FEB-1995	28.0	0.039	0.021	64^{+51}_{-41}
46	a127	9-MAR-1995	29.0	0.038	0.000	53^{+37}_{-26}
47	a128	7-APR-1995	26.0	0.030	0.000	25^{+32}_{-20}
48	a129	3-MAY-1995	28.0	0.067	0.036	7^{+42}_{-32}
49	a131	1-JUN-1995	27.0	0.042	0.016	90^{+62}_{-48}
50	a132	28-JUN-1995	28.0	0.058	0.017	55^{+51}_{-38}
51	a133	26-JUL-1995	28.0	0.014	0.000	29^{+32}_{-20}
52	a135	24-AUG-1995	20.0	0.010	0.020	27^{+36}_{-25}
53	a136	13-SEP-1995	21.0	0.027	0.013	56^{+44}_{-34}

GALLEX IV		Exposure		pulse shape analysis		
Runs		start	duration (d)	b_L	b_K	P_\odot (SNU)
54	a146	14-FEB-1996	21.0	0.135	0.015	104^{+61}_{-48}
55	a148	7-MAR-1996	22.0	0.010	0.053	47^{+62}_{-48}
56	a149	29-MAR-1996	19.0	0.053	0.012	60^{+55}_{-40}
57	a151	18-APR-1996	20.0	0.019	0.033	28^{+60}_{-40}
58	a157	27-JUN-1996	20.0	0.063	0.020	68^{+65}_{-50}
59	a158	17-JUL-1996	21.0	0.025	0.019	91^{+68}_{-52}
60	a161	29-AUG-1996	20.0	0.105	0.061	-98^{+52}_{-43}
61	a162	18-SEP-1996	22.0	0.041	0.000	100^{+59}_{-44}
62	a163	10-OCT-1996	41.0	0.062	0.012	125^{+59}_{-49}
63	a165	21-NOV-1996	20.0	0.024	0.009	106^{+65}_{-51}
64	a166	11-DEC-1996	29.0	0.053	0.000	201^{+69}_{-58}
65	a167	9-JAN-1997	13.0	0.025	0.015	82^{+64}_{-47}

Table 4: Single solar run results with stat. error (1σ) for GALLEX III and IV.

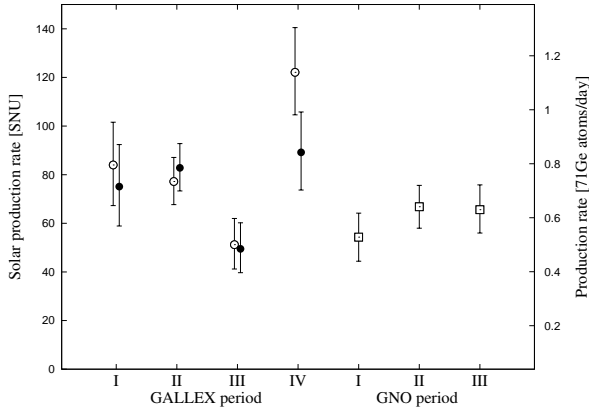


Figure 6: Results of the GALLEX periods (rise time (○) and pulse shape analysis (●)) compared to the three GNO periods (□).

periods I, II and III are in good agreement, the difference for period IV is remarkable. The statistical error bars have a small overlap, but one should keep in mind that both results were derived from the same data set and should be strongly correlated. To estimate the correlation in a quantitative way we compared the single run results of the periods I, II and III. The correlation coefficient $r_{x,y}$ is defined as

$$r_{xy} = \frac{\text{cov}(x, y)}{\sigma_x \sigma_y} \quad (6)$$

with the covariance

$$\text{cov}(x, y) = \frac{1}{n-1} \sum_{i=1}^n (x_i - \bar{x})(y_i - \bar{y}). \quad (7)$$

One gets $r_{xy} = 0.826$ and therefore $r_{x,y}^2 = 0.682$, where the latter is conventionally interpreted as the part of the variance of x caused by changes in y (and vice versa). If one applies this expectation to the GALLEX IV results, only a third of the variation is caused by statistical fluctuations. From this point of view the difference between the two results is very unlikely.

Concerning the rise time results it was already noted in [1][21] that the scattering of the four results is unusual. A χ^2 -test for compatibility with a constant mean yields a probability of less than 1% ($\chi^2 = 12.7$ with 3 degrees of freedom, assuming symmetric errors). However, it was shown that the scattering is decreased if different kinds of grouping are applied (e.g. four random divisions) resulting in probabilities up to 26.7%. For the results obtained by pulse shape analysis one calculates $\chi^2 = 7.1$ corresponding to a probability of 7%, mainly due to the lower GALLEX IV value.

As already discussed in [1] eight of the twelve runs of the GALLEX IV period had problems with electronic

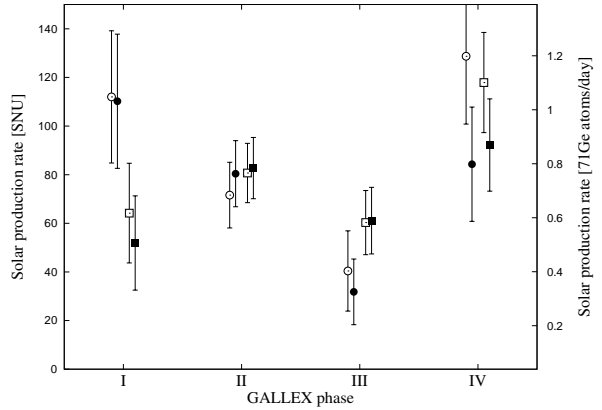


Figure 7: Independent analysis for L (○, ●) and K (□, ■) events with rise time and pulse shape method, respectively.

noise, which led to a missing baseline in case of low energy (L) events. While the uncertainty of the rise time determination increases, the evaluation of pulse shape parameters described in section 2 is not or only weakly affected by the location of the baseline level. However, a separate analysis of L and K events reveals that the high GALLEX IV result obtained with the rise time method cannot exclusively be assigned to the L events (see figure 7).

The event selection with the pulse shape analysis is more stringent compared to the rise time analysis, therefore it provides a better background reduction (see Figure 9) at the cost of a lower cut efficiency especially for K events. The diagram in Figure 8 shows the number of events selected by both types of analysis for GALLEX IV. The difference in the number of accepted K events is as expected, but it is remarkable that the number of accepted L events is almost equal. Therefore, the lower GALLEX IV result is caused by the time distribution of accepted events.

3.4. Combination with GNO

After the end of GALLEX the gallium neutrino observation at LNGS was continued by the GNO collaboration that performed 58 solar runs between 1998 and 2003

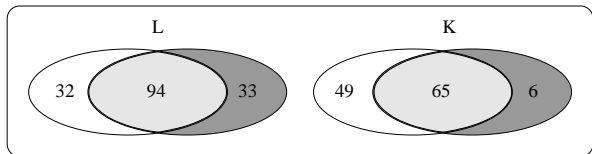


Figure 8: Number of selected GALLEX IV events with rise time (white) and pulse shape (grey) analysis for L and K energy region.

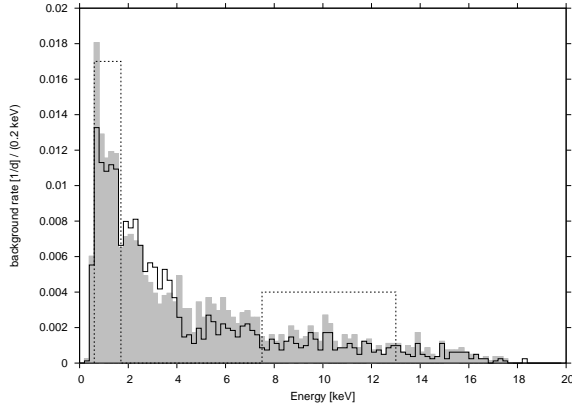


Figure 9: Background spectrum after pulse shape cut (black line) and rise time cut (grey). The energy regions of interest (L and K) are shown schematically with dashed boxes.

Fit	m	c	χ^2	d.o.f	p
$y(t) = c$		66.4	9.44	6	15.0%
$y(t) = m\bar{t} + c$	-1.08	66.4	8.55	5	12.8%

Table 5: χ^2 -fits to the seven GALLEX-GNO periods for both a constant and a linear dependence (where \bar{t} is the average time).

[6][7]. The experimental setup was basically the same as for GALLEX except for the electronics, which had been redesigned in order to replace and modernise the GALLEX counting system. The event selection was based on a pulse shape analysis in which a theoretical pulse shape was fitted to the measured pulse. A neural network trained by a large amount of reference events decided on the basis of the fit parameters whether an event was accepted or rejected [22].

The results of the three GNO measuring periods are shown in Figure 6 together with the four GALLEX periods. A χ^2 -test for compatibility with a constant mean yields $\chi^2 = 9.45$ corresponding to a probability of 15.0% (6 degrees of freedom). Since the GNO results seems to have a tendency to smaller values, we have also performed a linear fit to all seven GALLEX-GNO periods, but there was no improvement (the probability even decreased, see Table 5 and Figure 10).

The total GNO result is

$$P_{\odot} = \left[62.9_{-5.3}^{+5.5} (\text{stat.}) \pm 2.5 (\text{syst.}) \right] \text{SNU} . \quad (8)$$

and a combination with the GALLEX pulse shape result from eq. 3 yields

$$P_{\odot} = \left[67.6 \pm 4.0 (\text{stat.}) \pm 3.2 (\text{syst.}) \right] \text{SNU} . \quad (9)$$

The combination was calculated as a weighted mean using the statistical errors (with the approximation of

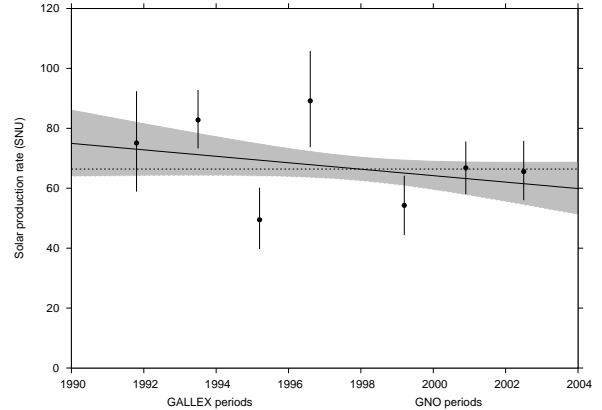


Figure 10: Constant and linear fit to the GALLEX-GNO periods with 1σ error region for the linear fit (grey).

symmetry). The systematic error was obtained by a quadratic combination of both single errors.

4. Source experiments

For a complete test of the experimental performance the GALLEX collaboration arranged two source experiments [15][16] in between the solar periods II-III and III-IV respectively. Two intense ^{51}Cr neutrino sources were produced by neutron capture on ^{50}Cr by irradiation of isotopically enriched chromium in the core of the Siloé reactor in Grenoble. The energies of the emitted neutrinos are about 750 keV (90%) and 430 keV (10%). For an accurate knowledge of the source activities A the latter were determined by different methods (for details see [16]). With the theoretical capture cross section of gallium $\sigma = 58.1_{-1.6}^{+2.1} \times 10^{-46} \text{cm}^2$ [23] one can predict the expected neutrino signal to compare it with the measurement. The sources were placed in a tube inside the gallium tank for exposure times of a few days up to 4 weeks. Else, the experimental procedure was the same as for solar runs.

Compared to the previous published results in [16], the reanalysis of the source experiments considers the following changes:

- new counter efficiencies due to more precise calibrations (6 of 18 source runs were affected).
- the update of the solar production rate by the combined result of GALLEX + GNO, which has to be treated as additional side reaction in the source experiments.
- event selection with pulse shape analysis instead of rise time. For an easier comparison the rise time results are given, too.

Run	date	rise time P [1/d]	pulse shape P [1/d]	
1	s107	23-JUN-1994	11.2 ^{+3.3} _{-2.9}	12.9 ^{+3.4} _{-3.0}
2	s108	27-JUN-1994	11.7 ^{+2.9} _{-2.6}	9.9 ^{+2.8} _{-2.4}
3	s109	1-JUL-1994	8.3 ^{+2.4} _{-2.2}	8.1 ^{+2.5} _{-2.2}
4	s110	6-JUL-1994	8.1 ^{+2.0} _{-1.8}	8.2 ^{+2.0} _{-1.8}
5	s111	13-JUL-1994	6.8 ^{+2.0} _{-1.7}	7.5 ^{+2.0} _{-1.8}
6	s112	20-JUL-1994	3.9 ^{+1.6} _{-1.4}	3.8 ^{+1.5} _{-1.3}
7	s113	27-JUL-1994	5.1 ^{+1.4} _{-1.3}	4.5 ^{+1.4} _{-1.2}
8	s114	9-AUG-1994	2.8 ^{+1.3} _{-1.1}	2.2 ^{+1.2} _{-1.0}
9	s115	24-AUG-1994	3.1 ^{+1.2} _{-1.1}	1.8 ^{+1.1} _{-0.9}
10	s116	7-SEP-1994	0.3 ^{+0.7} _{-0.5}	0.3 ^{+0.7} _{-0.5}
11	s117	28-SEP-1994	1.8 ^{+1.0} _{-0.8}	1.6 ^{+1.0} _{-0.8}
combined source exp. 1: $P(t=0)$		11.7 ± 1.1	11.2 ± 1.1	
1	s138	5-OCT-1995	9.8 ^{+3.0} _{-2.6}	9.7 ^{+3.1} _{-2.6}
2	s139	9-OCT-1995	9.2 ^{+2.8} _{-2.5}	9.4 ^{+2.9} _{-2.6}
3	s140	13-OCT-1995	7.0 ^{+1.4} _{-1.2}	6.9 ^{+1.4} _{-1.3}
4	s141	1-NOV-1995	5.8 ^{+1.3} _{-1.2}	5.6 ^{+1.4} _{-1.2}
5	s142	22-NOV-1995	2.0 ^{+1.1} _{-1.0}	2.2 ^{+1.1} _{-0.9}
6	s143	20-DEC-1995	1.6 ^{+1.0} _{-0.8}	2.0 ^{+0.9} _{-0.8}
7	s144	17-JAN-1996	1.5 ^{+0.9} _{-0.8}	1.5 ^{+0.9} _{-0.8}
combined source exp. 2: $P(t=0)$		10.4 ^{+1.2} _{-1.1}	10.5 ± 1.2	

Table 6: Results of single runs of both GALLEX ^{51}Cr source experiments expressed as production rate $P(t=0)$ at the beginning of each run. Errors are 1σ (statistical only).

The analysis procedure is the same as for the solar runs except for the time dependence of the source activity. The ^{51}Cr half-life of 27.7 d has to be considered in the likelihood function. The single run results are listed in Table 6. The time scale refers to the end of bombardment of source production, which is also the zero time for the combined analysis of all runs. The resulting source induced production rates R are given in Table 6, too. The corresponding source activities A^ν can be obtained by considering the cross section, the geometry of the gallium tank and the source positions [16] by

$$R_1(t) = 0.1856 A_1^\nu(t), \quad R_2(t) = 0.1866 A_2^\nu(t) \quad (10)$$

where the unit of R is 1/d if A is given in PBq. They are listed in Table 7 together with the ratio r of A^ν to the expected source activity A .

4.1. Discussion of the source experiments

We know from the ^{71}As experiment performed at the end of GALLEX that the Ge extraction yield is very close to 100%. Since the ground-state to ground-state cross section is known to within 1%, this implies that the two ^{51}Cr source experiments performed in GALLEX

	A^ν [PBq]	$r = A^\nu/A$	r [16]
source 1	63.4 ^{+1.1} _{-1.6}		
rise time	63.2 ^{+6.7} _{-6.5}	0.997 ^{+0.11} _{-0.11}	1.01 ^{+0.12} _{-0.11}
pulse shape	60.4 ^{+6.6} _{-6.3}	0.953 ^{+0.11} _{-0.11}	
source 2	69.1 ^{+3.3} _{-2.1}		
rise time	55.8 ^{+6.8} _{-6.6}	0.807 ^{+0.11} _{-0.10}	0.84 ^{+0.12} _{-0.11}
pulse shape	56.1 ^{+7.0} _{-6.7}	0.812 ^{+0.10} _{-0.11}	
rise time	0.902 ± 0.078		0.93 ± 0.08
pulse shape	0.882 ± 0.078		

Table 7: Results A^ν of the source experiments compared to the expected source activity A (both referring to the end of bombardment of the source production). For comparison, the last column gives the results as published before the present reanalysis.

have measured the contribution of the first two excited states in ^{71}Ge to the ^{71}Ga neutrino capture cross section. Reanalysing the data from these two source experiments using the pulse shape discrimination and improved counting efficiencies yields $r = 0.882 \pm 0.078$ (see Table 7). This ratio is 1.5σ away from the expectation value 1.0 where a 5% contribution from the first two excited states is included.

If the results from the ^{51}Cr and ^{37}Ar source experiments performed in the frame of SAGE [24][25] are also included, the total ratio is 0.87 ± 0.06 (though an experiment equivalent to the GALLEX ^{71}As experiment has not been performed for SAGE). This low value indicates that the contribution of the first two excited states is rather small. This is in agreement with the finding by Hata and Haxton [26] that the assumed proportionality between (p,n) forward scattering cross sections and Gamow-Teller strength is not always valid for weaker GT transitions.

If it is adopted that the excited state contribution to the ^{51}Cr cross section is closer to 0% than to 5% as estimated by Bahcall, then this is also true for the ^7Be neutrino capture cross section where the assumed contribution is 6% according to Bahcall [23] (derived from the (p,n) experiments). As a consequence the ^7Be contribution of $34.8^{+4.8}_{-4.3}$ SNU [27] to the total solar neutrino capture (without oscillations) should be reduced to 32.7 SNU with a slightly reduced error.

Acknowledgements

We thank all members of the GALLEX Collaboration ([1]-[5]) for their respective contributions towards producing the GALLEX data.

References

- [1] GALLEX Collaboration, W. Hampel et al., *Physics Letters B* 447 (1999) 127-133.
- [2] GALLEX Collaboration, P. Anselmann et al., *Physics Letters B* 285 (1992) 376-389.
- [3] GALLEX Collaboration, P. Anselmann et al., *Physics Letters B* 314 (1993) 445-458.
- [4] GALLEX Collaboration, P. Anselmann et al., *Physics Letters B* 357 (1995) 237-247.
- [5] GALLEX Collaboration, W. Hampel et al., *Physics Letters B* 388 (1996) 384-396.
- [6] GNO Collaboration, M. Altmann et al., *Physics Letters B* 490 (2000) 16-26.
- [7] GNO Collaboration, M. Altmann et al., *Physics Letters B* 616 (2005) 174-190.
- [8] W. Hampel, L. P. Remsberg, *Physical Review C* 31 (1985) 666.
- [9] A. Urban, Ph. D. Thesis, Technische Universität München 1989.
- [10] U. Schanda, Ph. D. Thesis, Technische Universität München 1993.
- [11] M. Altmann, Ph. D. Thesis, Technische Universität München 1996.
- [12] M. Altmann, F. v. Feilitzsch, U. Schanda, *Nuclear Instruments and Methods in Physics Research A* 381 (1996) 398-412.
- [13] GALLEX Collaboration, W. Hampel et al., *Physics Letters B* 436 (1998) 158-173.
- [14] F. Kaether, Ph. D. Thesis, Universität Heidelberg 2007.
- [15] GALLEX Collaboration, P. Anselmann et al., *Physics Letters B* 342 (1995) 440-450.
- [16] GALLEX Collaboration, W. Hampel et al., *Physics Letters B* 420 (1998) 114-126.
- [17] F. Kaether, Master Thesis, Universität Heidelberg 2003.
- [18] B. T. Cleveland, *Nuclear Instruments and Methods* 214 (1983) 451-458.
- [19] M. Cribier et al., *Astroparticle Physics* 4 (1995) 23-32.
- [20] M. Cribier et al., *Astroparticle Physics* 6 (1997) 129-141.
- [21] T. Kirsten, *Nuclear Physics B (Proc. Suppl.)* 77 (1999) 26-34.
- [22] L. Pandola, Ph. D. Thesis, Università degli Studi dell'Aquila, 2004.
- [23] J. N. Bahcall, *Physical Review C* 56 (1997) 3391.
- [24] SAGE Collaboration, J. N. Abdurashitov et al., *Physical Review C* 60 (1999) 055801.
- [25] SAGE Collaboration, J. N. Abdurashitov et al., *Physical Review C* 73 (2006) 045805.
- [26] N. Hata, W. Haxton, *Physics Letters B* 353 (1995) 422-431.
- [27] J. N. Bahcall, C. Peña-Garay, *New Journal of Physics* 6 (2004) 63.